**Atmospheric
Chemistry
and Physics
Discussions**

Generation of free convection due to changes of the local circulation system

R. Eigenmann[1]**, S. Metzger**[1,*]**, and T. Foken**[1]

[1]Department of Micrometeorology, University of Bayreuth, Bayreuth, Germany
[*]now at: Institute for Meteorology and Climate Research – Atmospheric Environmental Research (IMK-IFU), Karlsruhe Institut of Technology, Garmisch-Partenkirchen, Germany

Abstract

Eddy-covariance and Sodar/RASS experimental measurement data of the COPS (Convective and Orographically-induced Precipitation Study) field campaign 2007 are used to investigate the generation of near-ground free convection events in the Kinzig valley, Black Forest, Southwest Germany. The measured high-quality turbulent flux data revealed free convection to be induced in situations where high buoyancy fluxes and a simultaneously occurring wind speed collapse were present. The minimum in wind speed – observable by the Sodar measurements through the whole vertical extension of the valley atmosphere – is the consequence of a thermally-induced valley wind system, which changes its wind direction from down to up-valley winds in the morning hours. Buoyant forces then dominate over shear forces within turbulence production. These situations are detected by the stability parameter (ratio of the measurement height to the Obukhov length) calculated from directly measured turbulent fluxes. An analysis of the scales of turbulent motions during the free convection event using wavelet transform confirms the large-eddy scale character of the detected plume-like coherent structures. Regarding the entire COPS measurement period, free convection events (FCEs) in the morning hours occur on about 50% of all days.

1 Introduction

The COPS (Convective and Orographically-induced Precipitation Study) field campaign has been carried out from 1 June to 31 August 2007 within the low mountain range of the Black Forest, the Vosges Mountains and the Swabian Jura with the Rhine rift valley as a pronounced topographic lowland plain in between, thus setting the stage for studying the convection initiation processes and development of clouds and precipitation within complex terrain generated by both landscape heterogeneity and orographical structuring (Wulfmeyer et al., 2008). Rainfall in the COPS area is characterized by subgrid-scale convection initiation (CI) processes, e.g. orographically or thermally-

induced local circulation systems, triggered by the complex terrain, thus complicating the exact modeling and forecast of precipitation events (Meißner et al., 2007; Barthlott et al., 2006). The problems of modeling convective clouds and precipitation – its time, amount and location – are the premature initiation of convection, the simulation of convective precipitation events as being too spatially widespread and the overestimation of precipitation on the windward compared to the lee side over low-mountain ranges, e.g. the Black Forest (Schwitalla et al., 2008).

The interaction of the land surface with the overlying atmosphere crucially affects the energy and water cycle over many temporal and spatial scales (Betts et al., 1996). The spatial distribution and patchiness of individual land use elements can have a strong impact on the atmospheric boundary layer (ABL) evolution and its thermodynamic structure, as changes of the surface energy budget directly influence the surface turbulent fluxes of moisture, momentum and heat, which act as the link between the atmosphere and the underlying soil-vegetation system (Pielke, 2001). Dynamical phenomena in the ABL can be related to altering surface characteristics, since gradients in sensible heat flux produced by evapotranspiration, albedo and soil property discontinuities induce local or secondary circulation systems (Segal and Arritt, 1992). Together with diurnal mountain winds developing over mountainous terrain (Whiteman, 1990), land surface-atmosphere interactions and the related physical processes within complex terrain are the key to the local occurrence and timing of the initiation of convection, cloud formation and precipitation (Hanesiak et al., 2004; Pielke, 2001; Chen and Avissar, 1994; Rabin et al., 1990; Banta, 1990, 1984; Raymond and Wilkening, 1980). Besides land-surface interactions and orography, mesoscale and synoptic scale settings are assumed to play an important role for convective processes (Wulfmeyer et al., 2007). Kottmeier et al. (2008) discusses several mechanisms relevant for the convection initiation (CI) process in the COPS region, i.e. (i) surface heating and low-level flow convergence; (ii) surface heating and moisture supply overcoming convective inhibition during latent and/or potential instability; or (iii) mid-tropospheric dynamical processes due to mesoscale convergence lines and forced mean vertical motion.

11369

Convection in general is defined as a vertical transport or mixing of air mass characteristics which results from turbulence providing energy, momentum and mass transport. It can be classified into free and forced convection (Foken, 2008b; Stull, 1988). Forced convection is present if air masses are driven by mechanical forces, for example by the wind field or by inhomogeneities of the underlying surface (topography). In contrast, the atmosphere is said to be in a state of free convection if the fluid is solely driven by density fluctuations resulting from small-scale temperature or humidity differences. Ascent of an air parcel will be initiated when it is warmer or moister compared to the surrounding air. Temperature differences develop in the daytime by strong solar heating of the ground resulting in a superadiabatic lapse rate in the surface layer (Stull, 1988). Triggered by the unstable layer adjacent to the ground, plumes, which are coherent structures of warm rising air, or thermals, which originate as merged plumes in the mixed layer (ML), can be formed. If enough moisture is present, the tops of the thermal structures might reach their lifting condensation level (LCL) and fair-weather clouds (shallow convection) or even thunderstorms with cumulonimbus clouds (deep convection) – given that the ascending air parcel reaches its level of free convection (LFC) and enough convective available potential energy (CAPE) is present – might occur (Stull, 1988). Consequently, surface-based dry convection is closely related to moist convection, because it supplies the upper portions of the boundary layer with heat and moisture, thus altering its thermodynamic structure, i.e. reducing its convective inhibition (CIN; Chaboureau et al., 2004), or it serves as a lifting mechanism, which releases potential instability in the boundary layer due to high surface sensible heat fluxes (Segal et al., 1995).

The present study is based on the recent finding of Mayer et al. (2008) that near-ground generated free convection events (FCEs) originating from a valley may lead to a strong and sudden ozone decrease at a mountain summit (Hohenpeissenberg) in the morning hours. In their study, the FCEs are triggered by a simultaneously occurring wind speed minimum facilitating the conditions for free convection. On about half of the days these wind speed minima could be attributed to the onset of Alpine Pumping

11370

in the alpine foreland (Lugauer and Winkler, 2005) associated with a change of wind direction causing a drop of the horizontal wind speed. Hence, other mesoscale or local circulation systems initiated by complex terrain – e.g. the well known slope and valley winds in the Black Forest mountains (Kossmann and Fiedler, 2000; Kalthoff et al., 2000) – are expected to trigger FCEs.

For that reason, this study aims at demonstrating the applicability of common flux measurement techniques, e.g. the eddy-covariance (EC) method, to the detection of vigorous vertical transport mechanisms such as the FCEs in experimental data obtained during the COPS field campaign in the Kinzig valley (Black Forest mountains), which was found in earlier studies (e.g., Meißner et al., 2007) to establish a pronounced diurnal thermally-induced valley wind system. Moreover, the processed turbulent flux data passing through a detailed quality assurance and control effort are used to select and describe these FCEs in detail.

2 Materials and methods

2.1 COPS energy balance and turbulence network

The COPS field campaign (1 June to 31 August 2007), initiated within the German 6-year Priority Program 1167 "Quantitative Precipitation Forecast PQP (Praecipitationis Quantitativae Predictio)" and funded by the German Science Foundation (DFG), aims to identify the physical and chemical processes responsible for the deficiencies in QPF (Quantitative Precipitation Forecast) over low-mountain regions and to advance the quality of forecasts of orographically induced convective precipitation by 4D observations and modeling of its life cycle (Wulfmeyer et al., 2007). Within COPS, the University of Bayreuth coordinates the energy balance network with the aim of providing continuous surface flux and other surface quantity data of the required high accuracy and quality for the scientific community in general, but particularly for the forcing and validation of applied mesoscale models. The network of six collaborating institutes op-

erated altogether 17 energy balance and turbulence stations distributed over the entire COPS region. One of them is used in this paper to demonstrate the near-ground generation of free convection due to changes of the local circulation system in the Kinzig valley.

2.2 Site description and experiment set-up

The energy balance and turbulence station under investigation in the present study is located in the Kinzig valley near Fußbach (48°22′7.8″ N, 8°1′21.2″ E, 178 m a.s.l.) on the western edge of the Black Forest. The Kinzig valley at Fußbach is oriented in a N-S direction, thus specifying the main wind direction, and has a valley width of about 1.3 km. Mountain crests in the immediate vicinity of the Fußbach site reach maximal values of about 450 m a.s.l. The energy balance and turbulence station consisted of a eddy-covariance tower and a soil and radiation measurement complex enabling the detection of all surface energy balance components. A land use map with an area of $1 \times 1 \, \text{km}^2$, and with the location of the eddy-covariance station indicated as a black cross in the middle of the map, is given in Fig. 1. Additionally, the position of the radiation and soil measurement complex is marked by a red cross. The target land use type was a corn field (see Fig. 1). Fetch distances of the eddy-covariance system depending on wind sector can be obtained from Table 1.

The turbulent flux measuring system (sampling rate: 20 Hz) measured turbulent fluxes of momentum, sensible and latent heat as well as carbon dioxide (CO_2) using a CSAT3 (Campbell Scientific, Inc.) sonic anemometer for recording the wind vector and the sonic temperature T_S and a LI-7500 (LI-COR Biosciences) open-path gas analyser for water vapor (H_2O) and CO_2 concentrations. Short-wave components of the net radiation were measured with a CM24 (Kipp&Zonen), and long-wave components with an Eppley PIR (Eppley Laboratory, Inc.). The measurement height of the eddy-covariance station (2.57–4.25 m) and the radiation measurement complex (1.96–4.13 m) was regularly adjusted to the rapidly growing corn field (0.15–2.9 m) in the course of the measurement period. The soil measurement complex recorded the soil

heat flux at 0.1 m depth with a HFP01SC (Hukseflux Thermal Sensors) heat flux plate, the soil temperature at 0.02, 0.05, 0.1 and 0.2 m depth with PT100 soil thermometers and the soil moisture at 0.05 and 0.2 m depth with a TRIME (IMKO GmbH) TDR probe.

In addition to the energy balance measurements, the ABL structure was detected near Fußbach (see gray cross in Fig. 1) by an acoustic and radioacoustic sounding system applying a phase array Doppler Sodar DSDPA.90-64 with a 1290 MHz RASS extension by Metek GmbH. It provided vertical profiles of wind velocity, fluctuation of the vertical wind speed and acoustic temperature with an averaging period of 10 min and a vertical resolution of 20 m. Furthermore, a pressure sensor P6520 (Ammonit) and a 9 m profile mast equipped at six different heights with F460 cup anemometers (Climatronics) and Frankenberger psychrometers were installed at the Fußbach site (blue cross in Fig. 1). The profile mast as well as the radiation and soil measurement complex all operated with a sampling rate of 1 Hz averaged to 1 min values stored in the logger. More detailed information about the measuring set-up and background data can be obtained from the COPS experiment documentation of the University of Bayreuth (Metzger et al., 2007).

2.3 Quality control effort and data flow

The eddy-covariance flux data measured at the Fußbach site was processed and quality controlled applying the latest micrometeorological post-field data processing standards (e.g., Mauder et al., 2006) in order to obtain a data set of the desired quality and accuracy, which can be utilized for further fundamental research. Accordingly, the turbulent flux raw data recorded with the eddy-covariance (EC) method was postprocessed with the comprehensive software package TK2 developed at the University of Bayreuth (Mauder and Foken, 2004), which comprises state of the art flux corrections and post-field quality control including tests on the fulfillment of integral turbulence characteristics (ITC) and stationarity (Foken and Wichura, 1996; Foken et al., 2004). The individual quality checks of the stationarity and ITC test can be combined according to Foken et al. (2004) to an overall quality rating scheme resulting in flags for each

turbulent flux ranging from 1 to 9, where flags of classes 1–3 can be used for fundamental research, classes 4–6 can still be applied to determine monthly or annual sums of fluxes, classes 7–8 have the function of rough orientation and class 9 should always be rejected.

Theoretical assumptions actually restrict the EC method to homogeneous terrain, but the increasing requirement for continuous monitoring of flux data (Aubinet et al., 2000; Baldocchi et al., 2001) forced the application of the EC method within highly structured terrain such as that in the COPS region. This step is supported by the development of a valuable site evaluation and characterisation approach (Göckede et al., 2004, 2006), which combines the flux data quality approach (Foken et al., 2004) with a forward Lagrangian footprint model (Rannik et al., 2000, 2003), able to identify site-specific spatial quality structures and the spatial representivity of the measured flux data in the context of the underlying land use distribution. This approach has been recently employed on sites of the CarboEurope network by Rebmann et al. (2005) and Göckede et al. (2008) and is used in this study – together with an internal boundary layer evaluation procedure – in order to obtain target land use type-representative turbulent flux data sets of the required high quality usable by the COPS community for further analysis. The check for possible internal boundary layers, which form as a consequence of changes of the underlying surface characteristics, is implemented by using the following fetch-height relation to roughly estimate the height of the new equilibrium layer δ depending on fetch x (Raabe, 1983; Jegede and Foken, 1999) neglecting weak stability effects (Savelyev and Taylor, 2005):

$$z_a \leq \delta = 0.3\sqrt{x} \tag{1}$$

The aerodynamic measurement height z_a should be lower than δ in order to guarantee that the EC measurement takes place within the new equilibrium layer establishing over the target land use type.

The flow chart displayed in Fig. 2 illustrates that the individual data processing steps performed in this study ultimately aim at the description and evaluation of the free con-

vection events (FCEs) in the Kinzig valley. Besides the quality control effort (TK2 flux calculation, footprint analysis, internal boundary layer evaluation) adapted to the eddy-covariance flux data as described above, the low-frequency radiation, soil, pressure and profile mast raw data have been quality-checked, averaged to 30 min values and visualized as Hovmøller-type plots. The Hovmøller-type plot visualizes processed values in a diurnal vs. annual resolution over the entire measurement period. Additionally, Fig. 2 indicates the processing of quality-checked and 10 min averaged plots of the Sodar/RASS raw data used in this study to evaluate the local valley circulation system in the Kinzig valley.

2.4 Spectral analysis

Spectral analysis methods are used in this paper to study the temporal scales of single free convection events (FCEs) detected by the quality-controlled turbulent flux measurements. Methods used are the continuous wavelet transform (CWT) and the computation of power spectra, both applied to the time series of eddy-covariance raw data of the vertical wind speed, the horizontal wind speed components and the sonic temperature from 05:00 to 13:00 UTC.

To prepare data for the CWT, the time series were block averaged from the original 20 Hz raw data to a sampling frequency of 0.5 Hz in order to drastically reduce computational time of the CWT without altering the results significantly (e.g., Thomas and Foken, 2005) as the decisive scales range in the order of several seconds to a few minutes. Subsequently, all block averaged time series apart from the vertical wind speed (no trend removal necessary) have been detrended using polynomial regression. The resulting high-pass filtered time series is obtained by substracting the fitted polynom from the block averaged time series. The residual time series is used for the calculation of the CWT using the Morlet wavelet. The CWT and plotting routine of the wavelet power spectra was done by using the software package SOWAS (software for wavelet spectral analysis and synthesis: Maraun and Kurths, 2004; Maraun et al., 2007) implemented in the statistical computing software R. Results of a pointwise significance test

(significance level: 0.95) performed by Monte Carlo simulations (1000 realizations) are indicated by black solid lines in the plots of the wavelet power spectrum.

The calculation of the power spectra of detrended (by polynomial regression) and tapered 20 Hz time series of the vertical wind speed, the longitudinal wind speed and sonic temperature before, during and after the FCE period within the time range from 05:00 to 13:00 UTC was realized by applying a fast Fourier transform (FFT) to the computed autocorrelation function. Smoothing of the raw periodogram was performed using a modified Daniell smoother window technique.

3 Results and discussion

3.1 Quality control of the turbulent flux measurements

This section presents some results of the detailed quality control effort adapted to the eddy-covariance flux data as described in Sect. 2.3. Processed turbulent fluxes of sensible (Q_H) and latent heat (Q_E), friction velocity u_* as well as the CO_2 net ecosystem exchange NEE are depicted in Fig. 3 as Hovmøller-type plots where the color bar on the right side represents the calculated values with white areas indicating data failure (9.9% for each flux). Some results of the site evaluation approach using footprint analysis methods according to Göckede et al. (2004, 2006) are presented in Fig. 4. The footprint climatology for all flux measurements during stable atmospheric stratification in relation to the land use distribution (Fig. 4a) reveals good spatial representivity of the flux measurements, as the 5% effect level ring can be exclusively located within the target land use type "corn" intended to be measured (see also Fig. 1). As the extent of the footprint depends on atmospheric stratification and is enhanced with increasing stability, the depicted footprint climatology in Fig. 4a represents the average upper limit of possible extensions of the footprint. Generally, it has to be mentioned that the dimension of the footprint in our study is rather small, as it also depends on the aerodynamic measurement height, which at times did not exceed 2 m due to the

fast growing corn field (see Sect. 2.2). The spatial distribution of quality flags after Rebmann et al. (2005) of the momentum flux as related to the footprint climatology is illustrated in Fig. 4b. Here, the footprint climatology is depicted for all stratification regimes, thus being of smaller extent compared to that in Fig. 4a. It should also be noted that the quality flags of the attached color bar range from 1 to 5 and not from 1 to 9 as introduced in Sect. 2.3. The derivation of the flags after Rebmann et al. (2005) from the quality rating scheme after Foken et al. (2004) can be seen in Rebmann et al. (2005), where it is worth pointing out that in the case of flags after Rebmann et al. (2005), classes 1–2 are now suitable for fundamental research, classes 3–4 for the determination of monthly or annual sums of fluxes, and flux measurements flagged with class 5 have to be rejected. Referring to the quality ratings for the momentum flux in Fig. 4b, it is obvious that flags of class 1 and 2 can mainly be found within the 5% effect level ring indicating an overall good data quality. However, towards the valley sidewalls, in the eastern and western sectors, degraded data quality can be noted for the momentum flux. Similar patterns were found for Q_H, Q_E and CO_2 (not shown).

To gain insight into the average flux contribution over the entire measurement period of the target land use type "corn" as a function of different wind sectors and stability classes, appropriate sorted data have been individually processed within the footprint analysis procedure. The results are listed in Table 1 and reveal good average flux contributions of more than 92% for all wind sectors during unstable or neutral cases. However, for stable stratification easterly and westerly sectors have to be considered critically, as flux contributions below 80% can be found, with the minimum (67%) in the 240° wind sector. Admittedly, the latter finding has to be regarded with the knowledge that the density of available data is low in the easterly and westerly wind sectors as these do not lie within the main wind direction, thus weakening its influence on the overall assessment.

The results of the internal boundary layer evaluation of the eddy-covariance flux data as described in Sect. 2.3 are also depicted in Table 1, and are illustrative of average conditions over the entire measurement period and for the 12 wind sectors

distinguished. Referring to Table 1, the 270° sector shows a greater aerodynamic measurement height z_a compared to the height of the new equilibrium layer δ, thus indicating that the flux measurements within this sector cannot be associated with the target land use type "corn" regarding average conditions over the entire measurement period. Also the data of the 240° sector should be discarded, as δ is in the same range as z_a suggesting disturbed conditions.

However, it should be noted that the example of the average flux contribution calculation and the internal boundary layer evaluation presented in Table 1 only represent average conditions during the entire measurement period, as only an average canopy height of the corn field determining z_a and average fetch conditions have been assumed. The above described method could be adapted without any problems to shorter time periods, e.g. individual days, in order to get a better representation for single measurements. Nevertheless, the internal boundary layer evaluation in combination with the footprint analysis, both applied with average fetch conditions over the entire measurement period as an example in this paper (see Table 1), reveals sectors of less reliability and data quality, which can be excluded from further data analysis.

The energy balance closure – resulting from the aggregation of the turbulence and the radiation and soil data base (see Fig. 2) – is addressed in Fig. 5. Therefore, the sum of the turbulent fluxes Q_H and Q_E of each half-hourly measurement is plotted against the corresponding available energy values at the surface consisting of net radiation Q_S^* minus soil heat flux Q_G. The heat storage in the upper soil layer for the calculation of Q_G was considered applying the "simple measurement" (SM) method after Liebethal and Foken (2007). As the gray dashed line in Fig. 5 indicates a balanced energy exchange at the surface, one can deduce an average non-closure of 20.6% at the Fußbach site. The imbalance can primarily be attributed to the landscape heterogeneity assignable to the COPS region inducing unconsidered low-frequency flux contributions and advective flux components (Foken, 2008a; Foken et al., 2006). Indeed, large-eddy simulation (LES) studies recently revealed that turbulent organized structures (Kanda et al., 2004; Steinfeld et al., 2007) and secondary circulations (Inagaki et al., 2006) have an influ-

ence on the energy balance closure.

3.2   Generation of free convection at COPS IOP8b

The measurement of high-quality surface turbulent fluxes led to the detection of buoy-
antly driven free convection events (FCEs) in the morning hours, not only at the site
under investigation in this study (Fußbach), but also at other sites of the COPS energy
balance and turbulence network (Eigenmann, 2008). Preliminary graphics produced in
combination with routine data quality control during the COPS field phase consolidated
recently observed indications (Mayer et al., 2008) that thermally-driven circulation sys-
tems may trigger surface-induced free convection events in the morning hours, at times
when the existing circulation system changes its previously prevailed wind direction. In
the Kinzig valley a pronounced valley circulation system can frequently be observed to
be generated in high-pressure situations with high solar radiation and weak synoptic
forcing. At COPS IOP8b (15 July 2007) – outlined in this section as a paradigm for
the generation of FCEs at Fußbach – the Sodargramm of the wind direction in Fig. 6a
illustrates the ceasing of the down-valley, southerly winds which prevail at night and the
onset of up-valley, northerly blowing winds at about 08:30 UTC near the ground. Dur-
ing this transition period, a strong collapse of the horizontal wind speed through the
whole vertical extension of the valley atmosphere lasting from 06:50 until 08:50 UTC in
the morning hours, with values smaller than $1.5\,\mathrm{m\,s^{-1}}$, is evident from Sodar measure-
ments (Fig. 6b).

The occurrence of FCEs associated with the destabilization of near-ground air
masses can be detected by the EC flux measurements by calculating the stability pa-
rameter ζ according to the following equation:

$$\zeta = \frac{z}{L} = -\frac{z \cdot \kappa \cdot g \cdot \left(\overline{w'\theta_v'}\right)_0}{\overline{\theta_v} \cdot u_*^3} \tag{2}$$

where z denotes the measurement height, L the Obukhov length, u_* the friction veloc-

ity, g the acceleration due to gravity, $\overline{\theta_v}$ the mean virtual potential temperature, $\left(\overline{w'\theta_v'}\right)_0$
the buoyancy flux at the surface and κ the von-Kármán constant ($\kappa \approx 0.4$). Free con-
vection situations are indicated for $\zeta < -1$ (Foken, 2008b) and – regarding the equation
– will be facilitated for small values of u_* and high buoyancy fluxes, as buoyant forces
(B)

$$B = \frac{g}{\overline{\theta_v}} \cdot \left(\overline{w'\theta_v'}\right)_0 \tag{3}$$

then dominate over shear forces (S)

$$S = -\overline{u'w'} \cdot \frac{\partial \overline{u}}{\partial z} \tag{4}$$

within turbulence production, where S is the product of the momentum flux $\overline{u'w'}$ and
wind shear $\partial \overline{u}/\partial z$. Thus, the wind speed collapse in the valley (Fig. 6b) induced by
the wind direction change (Fig. 6a) provides a powerful trigger mechanism for FCEs.
In Fig. 7a, the stability parameter ζ is depicted, where the averaging period of the EC
flux measurements and the parameters deduced from them (Fig. 7a–g) was reduced
from the standard 30 min to 5 min in order to gain better insight into the temporal struc-
ture of the FCEs (see also Fig. 2). Events which had previously seemed to consist of
one single event within the 30 min resolution interval turned out to be an accumulation
of several convective pulses, of only a few minutes duration, transporting quantities
of heat and moisture into the ABL. Data quality is good during the event time, with
quality flags after Foken et al. (2004) ranging from 1 to 3 (see Sect. 2.3) within the
30 min data, 100% flux contribution from the target land use type "corn" and no dis-
turbance due to internal boundary layers. Referring to Fig. 7a, a vigorous event at
07:35–07:40 UTC with low values of ζ corresponds exactly to a 5 min duration local
minima of u_* ($0.04\,\mathrm{m\,s^{-1}}$) in Fig. 7d triggering the FCE. A second event, which can be
detected from 08:10–08:40 UTC, shows stability parameter values up to $\zeta = -1.4$ and

also coincides with a local minimum of u_* (0.09 m s^{-1}). Simultaneously, high values of Q_H (Fig. 7e) are found around the times of the FCEs (54.7 W m^{-2} at 08:25 UTC). Lower friction velocities u_* in general occur between 06:50 and 08:50 UTC explaining the generally small values of ζ in this time, thus indicating a whole period of destabilization of near-ground air masses and their subsequent vertical transport from 07:35 to 08:40 UTC (black dotted lines in Fig. 7a–i). In addition, Fig. 7i depicts the available energy at the ground ($-Q_S^* - Q_G$) for the portioning into Q_H (Fig. 7e) and Q_E (Fig. 7c), which can be expressed as the Bowen ratio Bo (Fig. 7f). Bo has its highest values (0.59 at 06:35 UTC) shortly before the free convection events demonstrating a preferred transformation of the available surface energy (daily max.: 590 W m^{-2} at 12:00 UTC) into Q_H.

Other parameters such as the ratio of the Deardorff velocity w_* (Deardorff, 1970a,b)

$$w_* = \left[\frac{g \cdot z_i}{\overline{\theta_v}} \cdot \left(\overline{w'\theta_v'} \right)_0 \right]^{1/3} \tag{5}$$

to the friction velocity u_* confirm their capability to denote FCEs (see Fig. 7g), where the depth of the boundary layer z_i is determined by visual inspection of a secondary maximum in the reflectivity profiles of the Sodar measurements (Beyrich, 1997). General difficulties in ABL determination within complex terrain (Staudt, 2006; Kalthoff et al., 1998; Kossmann et al., 1998) and the high background noise of the nearby street at the Fußbach measurement site complicate the evaluation of the Sodar data. On most days, no clear secondary maximum of reflectivity can be found for the daytime boundary layer evolution, thus making the determination of z_i a rough estimate rather than an exact determination. However, Fig. 6c shows the measured reflectivity of the Sodar/RASS complex, together with the determined evolution of z_i in the morning hours between 04:00–11:40 UTC indicated as black points, thus enabling the calculation of w_* and the subsequent display of $w_* \cdot u_*^{-1}$ in Fig. 7g at the same time.

Moreover, the ratio $B \cdot S^{-1}$ – calculated according to Eqs. (3) and (4) with the buoyant

11381

term B and the shear term S of the turbulence kinetic energy (TKE) equation – can be used to detect FCEs (see Fig. 7h). The wind shear $\partial \overline{u}/\partial z$, necessary for the calculation of S, was determined with the wind speeds measured with the cup anemometers at the profile mast at 4 and 9 m a.g.l. Considering a canopy height of 2.31 m at COPS IOP8b (15 July 2007) results in aerodynamic measurement heights z_a of 2.46 m and 7.46 m, respectively. The remarkable minima in Fig. 7h at the times of the FCE (07:35–08:40 UTC) underlines that the turbulence is mainly driven by buoyancy (B) rather than shear (S) forces. The chosen threshold of -3 (red dashed line in Fig. 7h) is chosen according to theoretical considerations in Stull (2000), which states favourable conditions for the generation of free convection for $|B| > |3 \cdot S|$.

So far parameters indicating the near-ground destabilization of surface-layer air masses have been presented, but the impact these FCEs exert on boundary layer thermodynamics and structure has not been discussed yet. As plume-like structures of rising air masses are a local phenomenon initiated by surface inhomogeneities, surrounded by areas of downdrafts and translated horizontally with the mean wind speed (Stull, 1988), it is not astonishing that the spatial as well as temporal averaged Sodar measurements (10 min averages) of the vertical wind speed only show slightly enhanced upward motions – greater than 0.2 m s^{-1} up to 140 m – during the FCE time (Fig. 6d). However, the onset of the first increased upward vertical wind speeds coincides well with the detected FCE period from 07:35–08:40 UTC regarding the daily cycle at COPS IOP8b. Moreover, it has to be mentioned that other COPS days, which show FCEs generated by a change of the local circulation system in the morning hours, exhibit stronger upward motions during the event time. As an example, the Sodargramms of the vertical wind speed at the high-pressure situations COPS IOP15a (12 August 2007) and IOP15b (13 August 2007) are shown in Fig. 6e and f, respectively, which both show strongly enhanced vertical wind speeds of locally more than 0.8 m s^{-1} through the whole vertical extension of the boundary layer during the times of lowered values of ζ in the morning hours.

Furthermore, the coherent structure of plume-like upward motions at COPS IOP8b

11382

can be assumed when regarding the turbulent time series of vertical wind speed, sonic temperature, humidity and carbon dioxide (not shown) as visual inspection of them during the FCE time clearly reveals ramp-like structures typical for coherent turbulent exchange (e.g., Gao et al., 1989; Bergström and Högström, 1989).

To explicitly demonstrate the large-eddy scale character of the FCE at COPS IOP8b, spectral analysis of the measured high-frequency turbulent time series (see Sect. 2.4) is utilized to reveal the scales of inherent turbulent eddies during the event time. Therefore, Fig. 8a and b show the wavelet power spectra of the vertical wind speed and sonic temperature, respectively, where the temporal section on the X-axis ranges from 05:00 to 13:00 UTC (480 min). It is obvious from the wavelet power spectra of the vertical wind speed (Fig. 8a), that during the FCE time (07:35–08:40 UTC) – marked by the black dotted vertical lines – a clear shift of significant areas of enhanced spectral power from high-frequency turbulence scales towards scales of lower frequency occurs. In particular scales in the range of 1 to 7 min experience an enormous gain in spectral power during the FCE period. These time scales can be associated with the time t_* it takes for air in plumes or thermals to cycle once between the bottom and the top of the ML which is stated, e.g. in Stull (1988), to range in the order of 5 to 15 min in the case of a well developed convective boundary layer (CBL). Considering the time of occurrence of the FCEs early in the morning hours within a growing boundary layer environment (see Fig. 6c), thus inhibiting larger circulation structures within this "early" CBL, our findings seem to be in good accordance with the textbook values. In our case, the average time scale $t_*=z_i \cdot w_*^{-1}$ during the FCE time (07:35–08:40 UTC) – calculated with an average z_i of 285 m (see Fig. 6c) and an average w_* of 0.75 m s^{-1} (see Fig. 7d and g; values of w_* in the order of 1 to 2 m s^{-1} are given, e.g. in Stull, 1988) – amounts to $t_*=6.3$ min.

Figure 8b also depicts the wavelet power spectrum of the sonic temperature, which shows a slightly different behavior compared to that of the vertical wind speed (Fig. 8a) discussed above. Spectral power during the FCE is also enhanced within scales in the range of 1 to 7 min (a second maximum can be found at around 13 min), but high-frequency turbulent scales are still present during the FCE period contrary to the finding

11383

in the wavelet power spectrum of the vertical wind speed. A possible explanation might be that the highly fluctuating temperature field close to the strongly heated surface causes a non-correlation between the wind and temperature field and, consequently, a different turbulent regime within the high-frequency part of the vertical wind speed and the temperature during the FCE time.

Spectral characteristics of the FCE at COPS IOP8b are further examined by plots of the computed power spectra (see Sect. 2.4) of the vertical wind speed (Fig. 9a–c), the longitudinal wind speed (Fig. 9d–f) and the sonic temperature (Fig. 9g–i), before (05:00–07:35 UTC), during (07:35–08:40 UTC) and after (08:40–13:00 UTC) the FCE period. All depicted spectra clearly reveal the existence of Kolmogorov's −5/3 power law (Kolmogorov, 1941) within a certain range in the inertial subrange. However, at lower frequencies, towards production scales, the shape of the spectra should depend on atmospheric stability as demonstrated, e.g. in Monin and Yaglom (1975, Chap. 8), with experimental results of Gurvich (1960, 1962) and Zubkovskii (1962), who found that wind velocity spectra satisfy the −5/3 power law over a certain region, but show a clear dependence on different values of the Richardson number at the lower limit of the inertial subrange. Similar experimental results have been reported, e.g. by Kaimal et al. (1972), who showed that normalized velocity and temperature spectra converge within the inertial subrange corresponding to Kolmogorov's power law, but spread out depending on ζ at the lower frequency part of the spectra. In accordance to the studies mentioned above, our computed spectra, especially that of the vertical (Fig. 9a–c) and longitudinal (Fig. 9d–f) wind speed, experience an appreciable gain of spectral power within time scales greater than 0.5 min during the FCE period (corresponding to low values of ζ) compared to the spectra before and after the FCE characterized by near-neutral conditions. Remarkable is the fact that the scale of maximal spectral power of the vertical wind speed during the FCE (Fig. 9b), which is found at about 4 min, coincides with the time scales of maximal power obvious in the wavelet power spectrum of the vertical wind speed (Fig. 8a). Moreover, the study of Katul et al. (1995) is used to gain more insight into the spectral characteristics within the low-frequency part of

11384

our spectra concerning a possible existence of a −1 power law and its deviation due to buoyancy. Katul et al. (1995) reported a −1 power law evident in the vertical and longitudinal wind speed and in the temperature power spectra during near-neutral atmospheric stratification, which can more or less be confirmed considering our spectra before and after the FCE (Fig. 9a, c, d, f, g, i) where neutral conditions are present. It has to be mentioned that the existence of a −1 power law for the vertical wind speed in the neutral case was found by Katul et al. (1995) to be only of limited extent (in accordance with our findings) and is also discussed, controversially, by Katul and Chu (1998). Considering now the behavior of the low-frequency spectral characteristics during the FCE period, it is noticeable that the existence of a −5/3 power law in the inertial subrange in the case of the vertical (Fig. 9b) and longitudinal (Fig. 9e) wind speed can be extended towards the production scales, which is also stated by Katul et al. (1995) for the free convection stability regime. In the case of the temperature power spectra Katul et al. (1995) referred to the existence of a −1/3 power law which can only be confirmed for a limited region, considering our temperature spectra (Fig. 9h). Finally, it is worthwhile to point out that our definition of the free convection regime ($\zeta < -1$) differs from that ($\zeta < -2$) used in Katul et al. (1995), so that the power laws corresponding to the case of moderately unstable conditions ($0.14 < \zeta < -1.3$) in the sense of Katul et al. (1995), i.e. a −2, a −1 and a −1 power law for the longitudinal and vertical wind speed and the temperature power spectra, respectively, may also be applied to our data, as average stability values during our FCE period ($\zeta = -1.3$) may also be associated with the upper edge of the moderately unstable regime of Katul et al. (1995). Nevertheless, to summarize our findings, the effect of buoyancy on the spectral characteristics of surface layer turbulence is clearly visible in our study.

Up to this point, the surface-induced generation of plume-like FCEs at COPS IOP8b and its spectral characteristics have been described in detail; now its contribution to possible cloud formation or even precipitation events over the COPS area shall be discussed. Satellite imagery (not depicted) did not reveal the formation of clouds over the Kinzig valley on that day. Nevertheless, the formation of some isolated fair-weather

11385

cumuli at COPS IOP8b, which can be associated with the FCEs, cannot be excluded but are not detectable using satellite imagery due to the sub-scale character of these clouds. Unfortunately, no cloud camera was installed near Fußbach. However, a single deep convective cell, which formed at COPS IOP8b in the vicinity of the upper Kinzig valley and is visible in radar data in Fig. 10, might have experienced a FCE-related contribution to its pre-convective environment, as vertically dislocated amounts of heat and moisture originating from the FCEs in the Kinzig valley might have been transported with the up-valley and synoptical winds towards the spot of onset of the cell. This assumption is supported if the eastward directed valley structure is considered to have been facilitating the large-scale flow dislocation due to channelling effects. Besides the FCE detected at Fußbach, the turbulence and energy balance station at Hagenbuch, which is located closer in relation to the convective cell as indicated in Fig. 10, also measured FCEs at COPS IOP8b.

3.3 Free convection events (FCEs) during the entire COPS measurement period

Having outlined the generation of FCEs due to a change of the valley wind system in detail for COPS IOP8b within the previous section, the entire measurement period should now be regarded. At Fußbach, 23 days, which make up 25% of the 92 days observed in the COPS field campaign, can be classified as "event days" coinciding with the paradigm of COPS IOP8b outlined in Sect. 3.2. Furthermore, 19 days (21%) can be denoted as "intermittent days", as they do not exhibit a clear diurnal, persistent valley wind circulation. FCEs occur but can only be attributed to brief duration – several minutes up to a few hours – changes from down-valley to up-valley winds during the day, these sometimes not even reaching a full wind rotation of 180°. Despite the fact that most of the FCEs of these "intermittent days" seem to be triggered by short changes of wind direction of varying duration, it was decided to separate the "intermittent" from the "event days" in order to have similar flow patterns initiating the FCEs and thus a clearly structured data set. The reason for the intermittence of the valley winds is a decrease of the solar energy input, e.g. due to cloud shading, which possibly could be ascribed

11386

to the formerly initiated free convection events in the morning hours providing the heat and moisture needed for the initiation of clouds. Finally, 37 days (40%) at Fußbach can be characterized as "non-event days", as FCEs were not accompanied by a valley wind rotation or in most cases did not actually appear. Thirteen days (14%) cannot be evaluated due to data failure.

Figure 11 shows all days classified as "event days" (23) with the onset and cessation times of the valley wind circulation system, the periods in which FCEs occurred and the times of sunrise and sunset valid for the COPS experiment period from June to August 2007. The mean onset and cessation times of the up-valley winds and the mean FCE times of those days classified as "event days", with standard deviation and number, are listed in Table 2 for the individual months and the whole measurement period. Remarkable is the adjustment of the onset of the up-valley winds and of the FCE times to the annual cycle of sunrise evident in the mean values of the individual months. The mean duration of the periods in which FCEs occur – depicted in Fig. 11 – is 1 h and 24 min with a standard deviation of 57 min.

To clarify the difference of "event" and "intermittent days" as related to the diurnal valley wind system, persistence values P were calculated from the EC sonic anemometer following Lugauer and Winkler (2005):

$$P(t) = \frac{\sqrt{\overline{u}(t)^2 + \overline{v}(t)^2}}{\overline{v_h(t)}} \qquad (6)$$

where the temporal vector mean of the horizontal wind speed is divided by the arithmetic mean of the horizontal wind speed at every time of the day. P can adopt values between 0 and 1, where 1 means that every day at that time the wind blew from the same direction. Figure 12a depicts the calculated persistence P for all days, "event days", "intermittent days" and "non-event days". Two pronounced eye-catching minima can be found for the "event days", i.e. one at the times the up-valley winds start (at about 08:00 UTC) and another at the times the up-valley winds rotate back to down-

valley winds (at about 18:00 UTC), indicating highly variable wind directions during these times. The P values above 0.75 for the rest of the time point to a quasi-identical flow pattern for the 23 selected "event days" at Fußbach. The small persistence values of the "intermittent days" between 06:00 and 18:00 UTC can be attributed to the non-persistence of the up-valley winds, as briefly lasting up-valley winds are interrupted by frequent rotations back to the original wind direction due to a decrease of the solar energy input (through cloud shading) which otherwise usually drives constantly blowing up-valley winds.

Mean diurnal courses of ζ (Fig. 12b), u_* (Fig. 12c), Q_H (Fig. 12d), global radiation (Fig. 12e) and Q_E (Fig. 12f) of the individually classified days can be applied to characterize the FCEs. Mean stability values ζ indicate the occurrence of FCEs in the morning hours at about 08:00 UTC for both "intermittent" and "event days". After this distinct minima of ζ at about 08:00 UTC (until about 12:00 UTC), the "intermittent days" show slightly lower ζ values, indicating that the intermittence of the valley wind system causes more frequent triggering of FCEs. A clear gap in the magnitude of u_* comparing "event" and "non-event days" during the minimum of ζ at about 08:00 UTC clarifies the capability of the morning hour valley wind transition period to generate FCEs. During the evening transition period at about 18:00 UTC values of u_* of the "event days" again fall below those of the "non-event days". The generally lower friction velocities for the "intermittent days" can be explained by the non-persistence of the valley winds resulting in a continuous drop of the horizontal wind speed. Above-average values of Q_H and global radiation (Fig. 12d and e) can be found for the "event days", thus indicating the preferred initiation of FCEs in clear, undisturbed weather situations with high solar radiation driving the valley winds, which act as the trigger mechanism for the FCEs by providing the necessary minimum of u_* in the early morning transition period. Moreover, about 100 W m^{-2} higher Q_E values (Fig. 12f) can be observed for the "event days" compared to the "non-event days", which also contribute, due to density effects, to the destabilization of near-ground air masses and, if mixed into the ML, may support cloud formation. The formation of fair-weather cumuli on "event days" at around mid-

day due to surface-induced convective transport mechanisms may be deduced from the depicted global radiation (Fig. 12e), as a drop from about 11:00 until 12:30 UTC deviates from the more or less bell-shaped course of the global radiation for the rest of the day.

4 Conclusions

A comprehensive quality assurance and control effort, including footprint analysis and a check for internal boundary layers, was adapted to the energy exchange measurements of the energy balance station at Fußbach incorporated in the COPS energy balance and turbulence network in order to obtain high-quality surface flux data usable for further analysis. The energy exchange measurements led to the detection and description of free convection events (FCEs) in the morning hours, which were found to be triggered by a change of the local circulation system in the Kinzig valley. These FCEs occurred on about half of the total 92 days investigated during the COPS field campaign summing up days classified as "event" and "intermittent days". This frequent occurrence of FCEs confirms the assumption of Mayer et al. (2008) that other regions showing complex terrain – besides the alpine foreland investigated in their study – might face trigger mechanisms, such as local or mesoscale circulation systems leading to the convective release of near-ground air masses into the ABL. FCEs initiated by a change of the valley winds were also found by Hiller et al. (2008) in an alpine valley in Switzerland following their stability and data quality analysis. Unfortunately, these authors did not address these events. Eddy-covariance measurement systems and the thereof derived stability parameter ζ, which indicates free convection situations for $\zeta < -1$, are able to detect such FCEs induced by local minima of the friction velocity u_* during the period of transition of the down-valley winds prevailing at night towards up-valley winds in the early morning hours. Other parameters such as the ratio of the Deardorff velocity w_* to the friction velocity u_* and the ratio of $B{\cdot}S^{-1}$ have been deduced in this study and confirm their capability to denote FCEs. The large-eddy scale

character of the FCEs could be confirmed applying spectral analysis methods, thus reinforcing the fact that FCEs are plume-like coherent structures of rising air masses transporting quantities of heat and moisture into the ABL and, consequently, may have a strong contribution to subsequent possible cloud formation and precipitation over the COPS region by altering ABL thermodynamics and structure. A contribution of the FCEs originating from the Kinzig valley to the pre-convective environment of the single convective cell, which developed in close proximity to the upper Kinzig valley at COPS IOP8b, has been speculated upon in the present study (see Fig. 10). To sum up, FCEs are likely – in addition to other orographic or landscape effects triggering convection – to have a non-negligible impact on ABL temperature and moisture profiles and to play a key role for CI processes. However, it must be noted that the measuring set-up with single turbulence point measurements cannot clarify the dimension and magnitude of the FCEs. The exact spatial extent of such plume-like FCEs remains unclear, as it cannot be assumed that they are spatially limited to the target land use type for which the turbulent fluxes are being measured. Consequently, it is not possible to clarify the horizontal dimensions of the near-ground air masses destabilized in the Kinzig valley and thus the exact quantities of heat and moisture transported upwards into the ABL. The application of up-scaling methods from target land use type-representative turbulent flux measurements towards landscape-scale incorporating conditions is desirable but is beyond the scope of this study. Moreover, the triggered turbulent pulse-like motions cannot be traced within the ABL, thus inhibiting detailed statements about the impact of these vertical transport mechanisms on local ABL thermodynamics and on possibly subsequent cloud formation. To address such questions, the application of a large-eddy simulation (LES) model in order to directly simulate the behavior of FCEs within the ABL would be desirable (e.g., Courault et al., 2007; Avissar and Schmidt, 1998). This could be supported by using the energy exchange measurements of this study to supply initial field and boundary conditions for the model. In the context of a follow-on project within the Priority Program 1167 "Quantitative Precipitation Forecast (PQP)", the application of LES will be utilized for further investigations.

References

Aubinet, M., Grelle, A., Ibrom, A., Rannik, U., Moncrieff, J., Foken, T., Kowalski, A. S., Martin, P. H., Berbiger, P., Bernhofer, C., Clement, R., Elbers, J. A., Granier, A., Grünwald, T., Morgenstern, K., Pilegaard, K., Rebmann, C., Snijders, W., Valentini, R., and Vesala, T.: Estimates of the Annual Net Carbon and Water Exchange of Forests The EUROFLUX Methodology, Adv. Ecol. Res., 30, 113–176, 2000. 11374

Avissar, R. and Schmidt, T.: An Evaluation of the Scale at which Ground-Surface Heat Flux Patchiness Affects the Convective Boundary Layer Using Large-Eddy Simulations, J. Atmos. Sci., 55, 2666–2689, 1998. 11390

Baldocchi, D., Falge, E., Gu, L. H., Olson, R., Hollinger, D., Running, S., Anthoni, P., Bernhofer, C., Davis, K., Evans, R., Fuentes, J., Goldstein, A., Katul, G., Law, B., Lee, X. H., Malhi, Y., Meyers, T., Munger, W., Oechel, W., U, K. T. P., Pilegaard, K., Schmid, H. P., Valentini, R., Verma, S., Vesala, T., Wilson, K., and Wofsy, S.: FLUXNET: A new tool to study the temporal and spatial variability of ecosystem-scale carbon dioxide, water vapor, and energy flux densities, B. Am. Meteorol. Soc., 82, 2415–2434, 2001. 11374

Banta, R. M.: Daytime Boundary-Layer Evolution over Mountainous Terrain. Part 1: Observations of the Dry Circulations, Mon. Weather Rev., 112, 340–356, 1984. 11369

Banta, R. M.: The role of mountain flows in making clouds, in: Atmospheric processes over complex terrain, edited by: Blumen, W., Meteorological monographs, 23(45), 229–283, American Meteorological Society, 1990. 11369

Barthlott, C., Corsmeier, U., Meißner, C., Braun, F., and Kottmeier, C.: The influence of mesoscale circulation systems on triggering convective cells over complex terrain, Atmos. Res., 81, 150–175, 2006. 11369

11391

Bergström, H. and Högström, U.: Turbulent exchange above a pine forest. II. Organized structures., Bound.-Lay. Meteorol., 49, 231–263, 1989. 11383

Betts, A. K., Ball, J. H., Beljaars, A. C. M., Miller, M. J., and Viterbo, P. A.: The land surface-atmosphere interaction: A review based on observational and global modeling perspectives, J. Geophys. Res.-Atmos., 101, 7209–7225, 1996. 11369

Beyrich, F.: Mixing height estimation from sodar data – A critical discussion, Atmos. Environ., 31, 3941–3953, 1997. 11381

Chaboureau, J. P., Guichard, F., Redelsperger, J. L., and Lafore, J. P.: The role of stability and moisture in the diurnal cycle of convection over land, Q. J. Roy. Meteorol. Soc., 130, 3105–3118, 2004. 11370

Chen, F. and Avissar, R.: Impact of Land-Surface Moisture Variability on Local Shallow Convective Cumulus and Precipitation in Large-Scale Models, J. Appl. Meteorol., 33, 1382–1401, 1994. 11369

Courault, D., Drobinski, P., Brunet, Y., Lacarrere, P., and Talbot, C.: Impact of surface heterogeneity on a buoyancy-driven convective boundary layer in light winds, Bound.-Lay. Meteorol., 124, 383–403, 2007. 11390

Deardorff, J. W.: Convective Velocity and Temperature Scales for the Unstable Planetary Boundary Layer and for Rayleigh Convection, J. Atmos. Sci., 27, 1211–1213, 1970a. 11381

Deardorff, J. W.: Preliminary Results from Numerical Integrations of the Unstable Planetary Boundary Layer, J. Atmos. Sci., 27, 1209–1211, 1970b. 11381

Eigenmann, R.: Investigation of conditions initiating free convection using energy exchange measurements. COPS-experiment, Black Forest, 2007, Master's thesis, University of Bayreuth, Germany, 2008. 11379

Foken, T.: The energy balance closure problem: An overview, Eco. Appl., 18, 1351–1367, 2008a. 11378

Foken, T.: Micrometeorology, Springer, 1st edn., New York, USA, 2008b. 11370, 11380

Foken, T. and Wichura, B.: Tools for quality assessment of surface-based flux measurements, Agr. Forest. Meteorol., 78, 83–107, 1996. 11373

Foken, T., Göckede, M., Mauder, M., Mahrt, L., Amiro, B. D., and Munger J. W.: Post-field data quality control, in: Handbook of Micrometeorology: A Guide for Surface Flux Measurement and Analysis, edited by: Lee, X., Massman, W., and Law, B., Kluwer, Dordrecht, The Netherlands, 181–208, 2004. 11373, 11374, 11377, 11380

Foken, T., Wimmer, F., Mauder, M., Thomas, C., and Liebethal, C.: Some aspects of the energy

11392

balance closure problem, Atmos. Chem. Phys., 6, 4395–4402, 2006, http://www.atmos-chem-phys.net/6/4395/2006/. 11378

Gao, W., Shaw, R. H., and Paw, U. K. T.: Observation of organized structures in turbulent flow within and above a forest canopy, Bound.-Lay. Meteorol., 47, 349–377, 1989. 11383

Göckede, M., Rebmann, C., and Foken, T.: A combination of quality assessment tools for eddy covariance measurements with footprint modelling for the characterisation of complex sites, Agr. Forest Meteorol., 127, 175–188, 2004. 11374, 11376

Göckede, M., Markkanen, T., Hasager, C. B., and Foken, T.: Update of a footprint-based approach for the characterisation of complex measurement sites, Bound.-Lay. Meteorol., 118, 635–655, 2006. 11374, 11376

Göckede, M., Foken, T., Aubinet, M., Aurela, M., Banza, J., Bernhofer, C., Bonnefond, J. M., Brunet, Y., Carrara, A., Clement, R., Dellwik, E., Elbers, J., Eugster, W., Fuhrer, J., Granier, A., Grünwald, T., Heinesch, B., Janssens, I. A., Knohl, A., Koeble, R., Laurila, T., Longdoz, B., Manca, G., Marek, M., Markkanen, T., Mateus, J., Matteucci, G., Mauder, M., Migliavacca, M., Minerbi, S., Moncrieff, J., Montagnani, L., Moors, E., Ourcival, J.-M., Papale, D., Pereira, J., Pilegaard, K., Pita, G., Rambal, S., Rebmann, C., Rodrigues, A., Rotenberg, E., Sanz, M. J., Sedlak, P., Seufert, G., Siebicke, L., Soussana, J. F., Valentini, R., Vesala, T., Verbeeck, H., and Yakir, D.: Quality control of CarboEurope flux data – Part 1: Coupling footprint analyses with flux data quality assessment to evaluate sites in forest ecosystems, Biogeosciences, 5, 433–450, 2008, http://www.biogeosciences.net/5/433/2008/. 11374

Gurvich, A. S.: Experimental investigation of frequency spectra of the vertical wind velocity in the atmospheric surface layer, Dokl. Akad. Nauk SSSR, 132, 1960. 11384

Gurvich, A. S.: Spectra of the vertical wind-velocity fluctuations and their relation to micrometeorological conditions, Atmospheric Turbulence, (Proc. In-ta Fiziki Atmosf. Akad. Nauk SSSR, No. 4), 101–136, 1962. 11384

Hanesiak, J. M., Raddatz, R. L., and Lobban, S.: Local initiation of deep convection on the Canadian prairie provinces, Bound.-Lay. Meteorol., 110, 455–470, 2004. 11369

Hiller, R., Zeeman, M. J., and Eugster, W.: Eddy-covariance flux measurements in the complex terrain of an Alpine valley in Switzerland, Bound.-Lay. Meteorol., 127, 449–467, 2008. 11389

Inagaki, A., Letzel, M. O., Raasch, S., and Kanda, M.: Impact of surface heterogeneity on energy imbalance: A study using LES, J. Meteorol. Soc. Jpn., 84, 187–198, 2006. 11378

Jegede, O. O. and Foken, T.: A study of the internal boundary layer due to a roughness change

in neutral conditions observed during the LINEX field campaigns, Theor. Appl. Climatol., 62, 31–41, 1999. 11374

Kaimal, J. C., Wyngaard, J. C., Izumi, Y., and Cote, O. R.: Spectral characteristics of surface-layer turbulence, Q. J. Roy. Meteorol. Soc., 98, 563–589, 1972. 11384

Kalthoff, N., Binder, H. J., Kossmann, M., Vogtlin, R., Corsmeier, U., Fiedler, F., and Schlager, H.: Temporal evolution and spatial variation of the boundary layer over complex terrain, Atmos. Environ., 32, 1179–1194, 1998. 11381

Kalthoff, N., Horlacher, V., Corsmeier, U., Volz Thomas, A., Kolahgar, B., Geiss, H., Mollmann Coers, M., and Knaps, A.: Influence of valley winds on transport and dispersion of airborne pollutants in the Freiburg-Schauinsland area, J. Geophys. Res.-Atmos., 105, 1585–1597, 2000. 11371

Kanda, M., Inagaki, A., Letzel, M. O., Raasch, S., and Watanabe, T.: LES study of the energy imbalance problem with Eddy covariance fluxes, Bound.-Lay. Meteorol., 110, 381–404, 2004. 11378

Katul, G. G. and Chu, C. R.: A theoretical and experimental investigation of energy-containing scales in the dynamic sublayer of boundary-layer flows, Bound.-Lay. Meteorol., 98, 279–312, 1998. 11385

Katul, G. G., Chu, C. R., Parlange, M. B., Albertson, J. D., and Ortenburger, T. A.: Low-wavenumber spectral characteristics of velocity and temperature in the atmospheric surface layer, J. Geophys. Res., 100, 14243–14255, 1995. 11384, 11385

Kolmogorov, A. N.: Rassejanie energii pri lokolno-isotropoi turbulentnosti, Dokl. AN. SSSR., 32, 22–24, 1941. 11384

Kossmann, M. and Fiedler, F.: Diurnal momentum budget analysis of thermally induced slope winds, Meteorol. Atmos. Phys., 75, 195–215, 2000. 11371

Kossmann, M., Vogtlin, R., Corsmeier, U., Vogel, B., Fiedler, F., Binder, H. J., Kalthoff, N., and Beyrich, F.: Aspects of the convective boundary layer structure over complex terrain, Atmos. Environ., 32, 1323–1348, 1998. 11381

Kottmeier, C., Kalthoff, N., Corsmeier, U., Barthlott, C., van Baelen, J., Behrendt A., Behrendt, R., Blyth, A., Coulter, R., Crewell, S., Dorninger, M., Foken, T., Hagen, M., Hauck, C., Höller, H., Konow, H., Kunz, M., Mahlke, H., Mobbs, S., Richard, E., Steinacker, R., Weckwerth, T., and Wulfmeyer, V.: Mechanisms initiating convection during the COPS experiment, Meteorol. Z., 17, 931–948, 2008. 11369

Liebethal, C. and Foken, T.: Evaluation of six parameterization approaches for the ground heat

flux, Theor. Appl. Climatol., 88, 43–56, 2007. 11378

Lugauer, M. and Winkler, P.: Thermal circulation in South Bavaria – climatology and synoptic aspects, Meteorol. Z., 14, 15–30, 2005. 11371, 11387

Maraun, D. and Kurths, J.: Cross Wavelet Analysis. Significance Testing and Pitfalls, Nonlinear Proc. Geoph., 11, 505–514, 2004. 11375

Maraun, D., Kurths, J., and Holschneider, M.: Nonstationary Gaussian Processes in Wavelet Domain: Synthesis, Estimation and Significance Testing, Phys. Rev. E., 75, 016707, doi:10.1103/PhysRevE.75.016707, 2007. 11375

Mauder, M. and Foken, T.: Documentation and instruction manual of the Eddy covariance software package TK2, Work Report University of Bayreuth, Department of Micrometeorology, 26, Print: ISSN 1614-8916, 42 pp., 2004. 11373

Mauder, M., Liebethal, C., Göckede, M., Leps, J. P., Beyrich, F., and Foken, T.: Processing and quality control of flux data during LITFASS-2003, Bound.-Lay. Meteorol., 121, 67–88, 2006. 11373

Mayer, J.-C., Staudt, K., Gilge, S., Meixner, F. X., and Foken, T.: The impact of free convection on late morning ozone decreases on an Alpine foreland mountain summit, Atmos. Chem. Phys., 8, 5941–5956, 2008, http://www.atmos-chem-phys.net/8/5941/2008/. 11370, 11379, 11389

Meißner, C., Kalthoff, N., Kunz, M., and Adrian, G.: Initiation of shallow convection in the Black Forest mountains, Atmos. Res., 86, 42–60, 2007. 11369, 11371

Metzger, S., Foken, T., Eigenmann, R., Kurtz, W., Serafimovich, A., Siebicke, L., Olesch, J., Staudt, K., and Lüers, J.: COPS experiment, Convective and orographically induced precipitation study, 01 June 2007–31 August 2007, Documentation, Work Report University of Bayreuth, Department of Micrometeorology, 34, Print: ISSN 1614-8916, 72 pp., 2007. 11373

Monin, A. S. and Yaglom, A. M.: Statistical Fluid Mechanics, Volume II: Mechanics of Turbulence, MIT Press, Cambridge, Massachusetts, and London, UK, 1975. 11384

Pielke, R. A.: Influence of the spatial distribution of vegetation and soils on the prediction of cumulus convective rainfall, Rev. Geophys., 39, 151–177, 2001. 11369

Raabe, A.: On the relation between the drag coefficient and fetch above the sea in the case of off-shore wind in the near-shore zone, Z. Meteorol., 33, 363–367, 1983. 11374

Rabin, R. M., Stadler, S., Wetzel, P. J., Stensrud, D. J., and Gregory, M.: Observed Effects of Landscape Variability on Convective Clouds, B. Am. Meteorol. Soc., 71, 272–280, 1990. 11369

Rannik, U., Aubinet, M., Kurbanmuradov, O., Sabelfeld, K. K., Markkanen, T., and Vesala, T.: Footprint analysis for measurements over a heterogeneous forest, Bound.-Lay. Meteorol., 97, 137–166, 2000. 11374

Rannik, U., Markkanen, T., Raittila, J., Hari, P., and Vesala, T.: Turbulence statistics inside and over forest: Influence on footprint prediction, Bound.-Lay. Meteorol., 109, 163–189, 2003. 11374

Raymond, D. and Wilkening, M.: Mountain-Induced Convection under Fair Weather Conditions, J. Atmos. Sci., 37, 2693–2706, 1980. 11369

Rebmann, C., Göckede, M., Foken, T., Aubinet, M., Aurela, M., Berbigier, P., Bernhofer, C., Buchmann, N., Carrara, A., Cescatti, A., Ceulemans, R., Clement, R., Elbers, J. A., Granier, A., Grunwald, T., Guyon, D., Havrankova, K., Heinesch, B., Knohl, A., Laurila, T., Longdoz, B., Marcolla, B., Markkanen, T., Miglietta, F., Moncrieff, J., Montagnani, L., Moors, E., Nardino, M., Ourcival, J. M., Rambal, S., Rannik, U., Rotenberg, E., Sedlak, P., Unterhuber, G., Vesala, T., and Yakir, D.: Quality analysis applied on eddy covariance measurements at complex forest sites using footprint modelling, Theor. Appl. Climatol., 80, 121–141, 2005. 11374, 11377, 11403

Savelyev, S. A. and Taylor, P. A.: Internal boundary layers: I. Height formulae for neutral and diabatic flows, Bound.-Lay. Meteorol., 115, 1–25, 2005. 11374

Schwitalla, T., Bauer, H.-S., Wulfmeyer, V., and Zaengl, G.: Systematic errors of QPF in low-mountain regions as revealed by MM5 simulations, Meteorol. Z., 17, 903–919, 2008. 11369

Segal, M. and Arritt, R. W.: Nonclassical mesoscale circulations caused by surface sensible heat-flux, B. Am. Meteorol. Soc., 73, 1593–1604, 1992. 11369

Segal, M., Arritt, R. W., Clark, C., Rabin, R., and Brown, J.: Scaling Evaluation of the Effect of Surface Characteristics on Potential for Deep Convection over Uniform Terrain, Mon. Weather Rev., 123, 383–400, 1995. 11370

Staudt, K.: Determination of the atmospheric boundary layer height in complex terrain during SALSA 2005, Master's thesis, University of Bayreuth, Germany, 2006. 11381

Steinfeld, G., Letzel, M. O., Raasch, S., Kanda, M., and Inagaki, A.: Spatial representativeness of single tower measurements and the imbalance problem with eddy-covariance fluxes: results of a large-eddy simulation study, Bound.-Lay. Meteorol., 123, 77–98, 2007. 11378

Stull, R. B.: An introduction to boundary layer meteorology, Atmospheric sciences library, Kluwer Academic Publishers, Dordrecht, The Netherlands, 1988. 11370, 11382, 11383

Stull, R. B.: Meteorology for scientists and engineers, Brooks/Cole, Pacific Grove, 2. edn.,

California, USA, 2000. 11382

Thomas, C. and Foken, T.: Detection of long-term coherent exchange over spruce forest using wavelet analysis, Theor. Appl. Climatol., 80, 91–104, 2005. 11375

Whiteman, C. D.: Observations of thermally developed wind systems in mountainous terrain, in: Atmospheric processes over complex terrain, edited by: Blumen, W., Meteorological monographs, 23(45), American Meteorological Society, Boston, Massachusetts, USA, 5–42, 1990. 11369

Wulfmeyer, V., Behrendt, A., Adrian, G., Althausen, D., Aoshima, F., van Baelen, J., Barthlott, C., Bauer, H. S., Blyth, A., Brandau, C., Corsmeier, U., Craig, G., Crewell, S., Dick, G., Dorninger, M., Dufournet, Y., Ehret, G., Engelmann, R., Flamant, C., Foken, T., Hauck, C., Girolamo, P. D., Graßl, H., Grzeschik, M., Handwerker, J., Hagen, M., Hardesty, R. M., Junkermann, W., Kalthoff, N., Kiemle, C., Kottmeier, C., Krauss, L., Long, C., Lelieveld, J., Madonna, F., Miller, M., Mobbs, S., Neininger, B., Pal, S., Peters, G., Radlach, M., Richard, E., Rotach, M., Russchenberg, H., Schlüssel, P., Schumann, U., Simmer, C., Steinacker, R., Turner, D., Vogt, S., Volkert, H., Weckwerth, T., Wernli, H., Wieser, A., and Wunraum, C.: Convective and Orographically-induced Precipitation Study. COPS Field Report 2.1., online available at: https://www.uni-hohenheim.de/spp-iop/documents/COPSFieldReport2. pdf, 2007. 11369, 11371

Wulfmeyer, V., Behrendt, A., Bauer, H.-S., Kottmeier, C., Corsmeier, U., Blyth, A., Craig, G., Schumann, U., Hagen, M., Crewell, S., Di Girolamo, P., Flamant, C., Miller, M., Montani, A., Mobbs, S., Richard, E., Rotach, M. W., Arpagaus, M., Russchenberg, H., Schluessel, P., Koenig, M., Gaertner, V., Steinacker, R., Dorninger, M., Turner, D. D., Weckwerth, T., Hense, A., and Simmer, C.: The Convective and Orographically-induced Precipitation Study: A Research and Development Project of the World Weather Research Program for Improving Quantitative Precipitation Forecasting in Low-Mountain Regions, B. Am. Meteorol. Soc., 89, 1477–1486, 2008. 11368

Zubkovskii, S. L.: Frequency spectra of the horizontal wind-velocity fluctuations in the atmospheric surface layer, Izv. Akad. Nauk SSSR, Ser. Geofiz, 10, 1425–1433, 1962. 11384

11397

Table 1. Average flux contribution [%] from the target land use type "corn" depending on wind sector and stability class at Fußbach. Moreover, the internal boundary layer evaluation procedure for average conditions over the entire measurement period is depicted. The internal boundary layer height δ calculated according to Eq. (1) with fetch x are listed in dependence of the 12 wind sectors distinguished. Wind sectors where δ falls below the average aerodynamic measurement height $z_a = 2.29$ m are flagged by "X".

	30°	60°	90°	120°	150°	180°	210°	240°	270°	300°	330°	360°
Average flux contribution from target land use type "corn" in %:												
Stable	92	77	82	86	86	89	86	67	73	69	84	89
Neutral	98	–	99	97	97	97	96	94	92	95	97	99
Unstable	99	100	100	100	100	99	99	99	99	99	99	100
Internal boundary layer evaluation:												
x [m]	141	83	68	84	113	102	89	59	49	66	101	162
δ [m]	3.56	2.73	2.47	2.75	3.19	3.03	2.83	2.30	2.10	2.44	3.01	3.82
z_a [m]					←	2.29	→		X			

11398

Table 2. Mean onset and cessation times [UTC] of the up-valley winds and the mean FCE times of those days classified as "event days", with standard deviation (SD), and number (n) for the individual months (June, July, August) and for the whole COPS measurement period at Fußbach.

Onset of up-valley wind				Cessation of up-valley wind				FCEs			
Period	Mean	SD	n	Period	Mean	SD	n	Period	Mean	SD	n
June	08:01	01:14	8	June	17:36	00:55	7	June	07:33	01:08	8
July	08:03	00:37	5	July	17:23	01:35	5	July	08:14	00:51	5
August	09:06	00:46	10	August	17:56	01:10	10	August	08:48	00:42	10
whole	08:29	01:02	23	whole	17:42	01:10	22	whole	08:14	01:01	23

11399
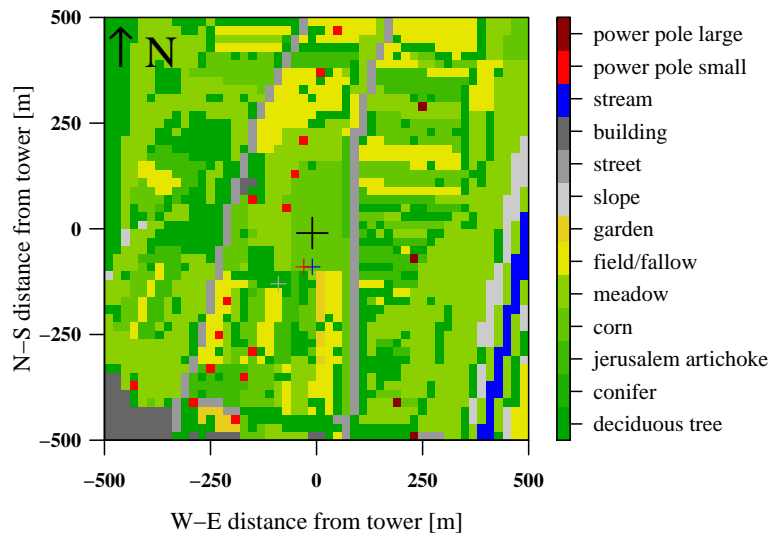
Fig. 1. Land use map ($1\times1\,km^2$) at the energy balance and turbulence station Fußbach with the location of the eddy-covariance station indicated as a black cross in the middle of the map. The additional crosses mark the position of the profile mast (blue), the radiation and soil measurement complex (red) and the Sodar/RASS system (gray). The target land use type of the eddy-covariance system, the radiation and soil measurement complex and the profile mast is a corn field. Fetch distances of the eddy-covariance system depending on wind sector can be obtained from Table 1.
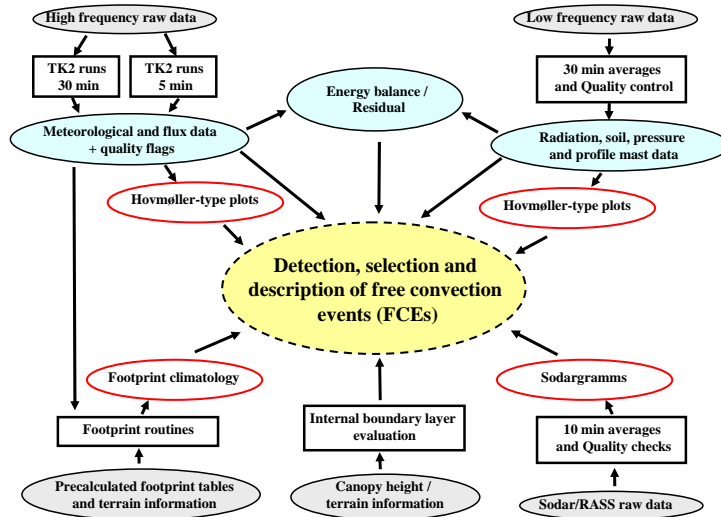
Fig. 2. Flow chart of individual data processing steps resulting in an overall assessment of the free convection events (FCEs) as being the main focus of this paper. Gray shaded ellipses display raw and input data for the processing steps indicated as black framed boxes. Blue shaded ellipses depict data bases emerging from the processing steps and red framed ellipses the graphical outputs.
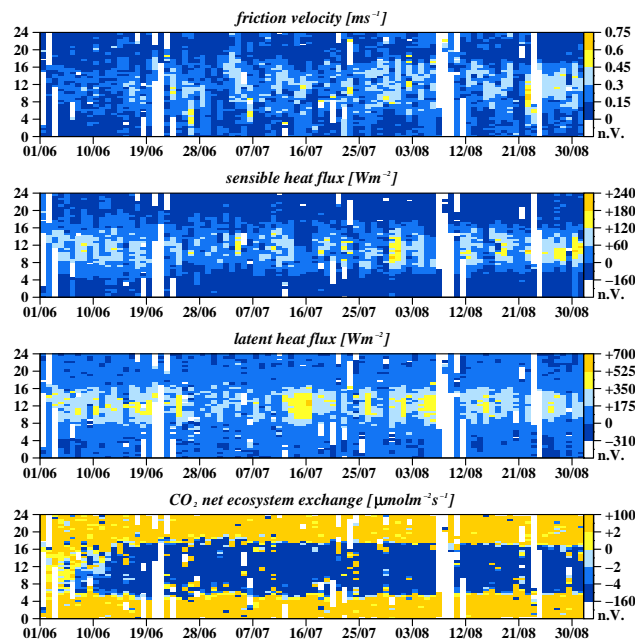
11401

Fig. 3. Friction velocity u_* $\left[\mathrm{m\,s^{-1}}\right]$, sensible heat flux Q_H $\left[\mathrm{W\,m^{-2}}\right]$, latent heat flux Q_E $\left[\mathrm{W\,m^{-2}}\right]$ and CO_2 NEE $\left[\mu\mathrm{mol\,m^{-2}\,s^{-1}}\right]$ for the entire COPS measurement period at Fußbach. X-axis represents the day of the year, Y-axis the time of the day [UTC] and the attached color bar the calculated values, where n.V. indicates data failure.
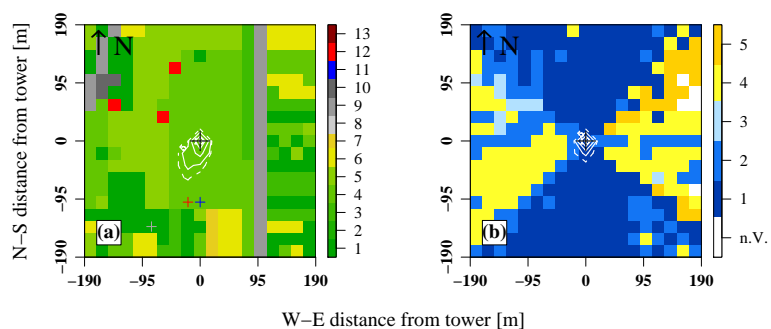
11402

Fig. 4. Land use classes **(a)** and quality ratings **(b)** as related to the footprint climatology at Fußbach. The footprint climatology on the left (a) is depicted only for all stable atmospheric conditions during the COPS measurement period; on the right side (b) all stratification regimes are included. The white contour lines indicate the 5% (dashed) and the 10, 30, 60, 90% (solid) effect level rings of the flux measurements. The eddy-covariance tower position is indicated by the central black cross. Land use classes in (a) are distinguished as follows (see also Fig. 1): deciduous tree (1), conifer (2), jerusalem artichoke (3), corn (4, target land use type), meadow (5), field/fallow (6), garden (7), slope (8), street (9), building (10), stream (11), power pole small (12) and power pole large (13). The quality flags distinguished in (b) range from 1 to 5, according to Rebmann et al. (2005), where n.V. indicates that no data are available for this cell.
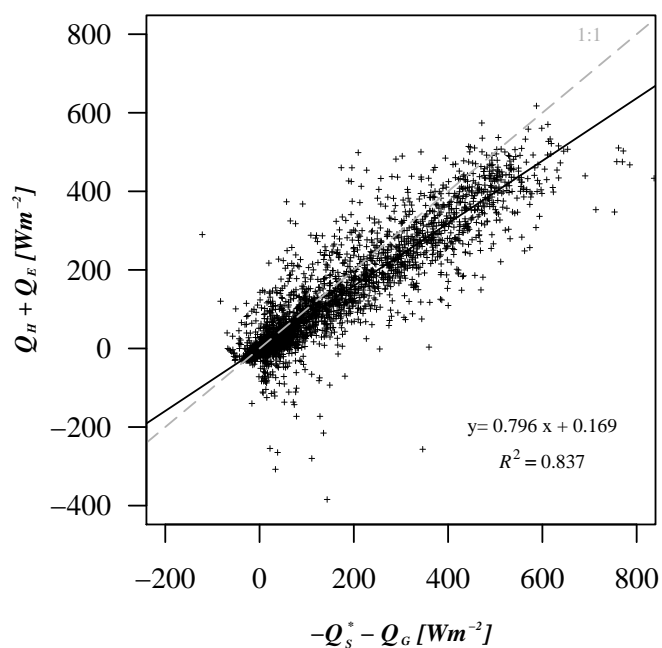
11403

Fig. 5. Relation between the available energy $-Q_S^* - Q_G$ $\left[\text{W m}^{-2}\right]$ (net radiation Q_S^* minus soil heat flux Q_G) at the surface and the sum of the both turbulent fluxes Q_H and Q_E $\left[\text{W m}^{-2}\right]$ at Fußbach. The regression equation and coefficient of the linear regression adapted to the scatter plot are also denoted. The gray dashed line indicates the 1:1-ratio.
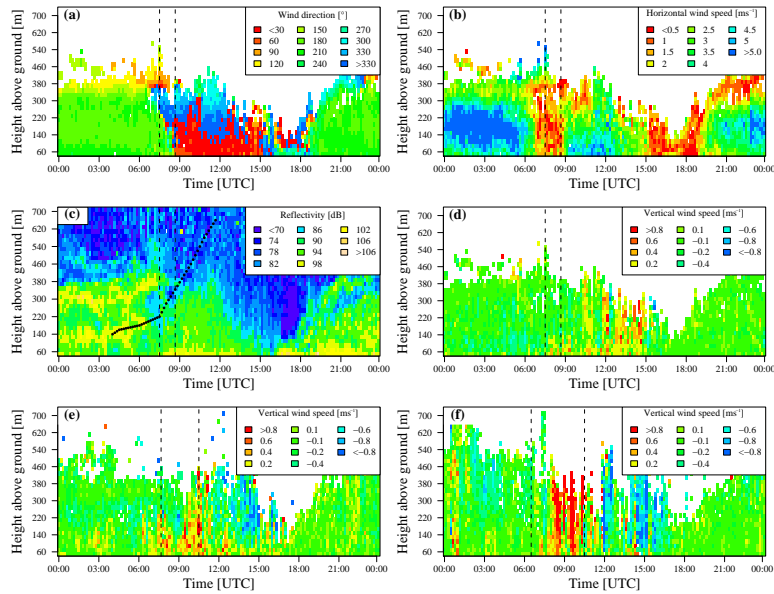
11404

Fig. 6. Sodargramms of the wind direction $[°]$ **(a)**, horizontal wind speed $\left[\text{m s}^{-1}\right]$ **(b)**, reflectivity [dB] **(c)** and vertical wind speed $\left[\text{m s}^{-1}\right]$ **(d)** for COPS IOP8b at Fußbach. Also plotted are the vertical wind speed $\left[\text{m s}^{-1}\right]$ for COPS IOP15a **(e)** and COPS IOP15b **(f)** at Fußbach. The black dashed lines in each figure indicate the period of low values of ζ in the morning hours: 07:35–08:40 UTC at IOP8b (see Fig. 6a), 07:45–10:35 UTC at IOP15a and 06:30–10:35 UTC at IOP15b. The black points in (c) represent the evolution of the boundary layer depth z_i between 04:00 and 11:40 UTC determined by visual inspection of a secondary maximum in the reflectivity profile.
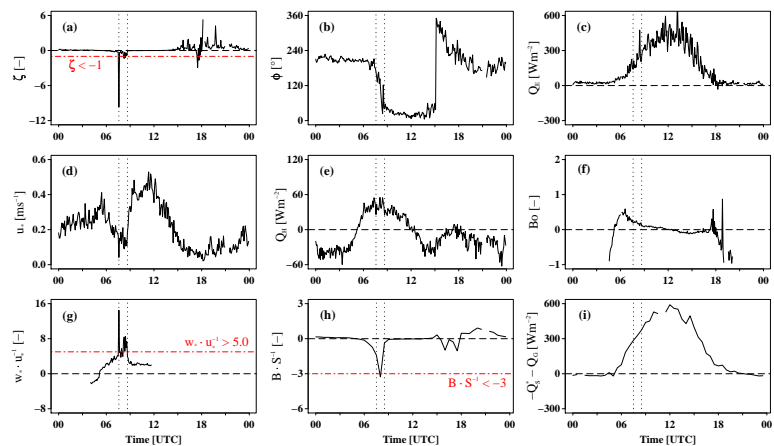
11405

Fig. 7. Stability parameter ζ [–] **(a)**, wind direction ϕ $[°]$ **(b)**, Q_E $\left[\text{W m}^{-2}\right]$ **(c)**, u_* $\left[\text{m s}^{-1}\right]$ **(d)**, Q_H $\left[\text{W m}^{-2}\right]$ **(e)**, Bo [–] **(f)**, $w_* \cdot u_*^{-1}$ [–] **(g)**, $B \cdot S^{-1}$ [–] **(h)** and available energy $-Q_S^* - Q_G$ $\left[\text{W m}^{-2}\right]$ **(i)** for COPS IOP8b at Fußbach. The black dotted lines in each graph indicate the period of destabilisation of near-ground air masses in the morning hours (07:35 UTC to 08:40 UTC) due to low values of ζ.

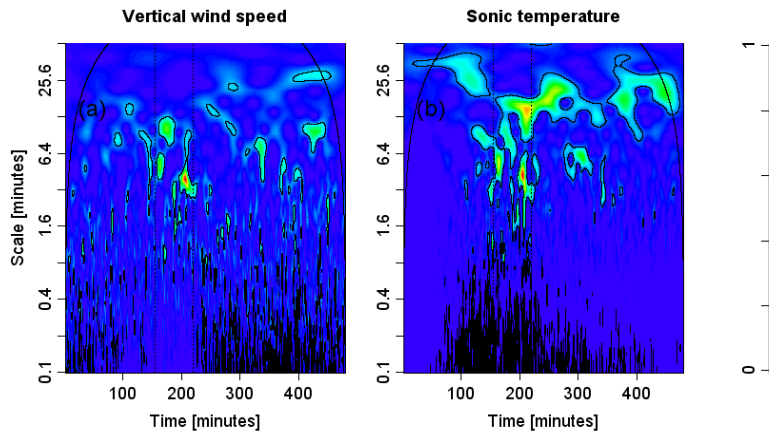11406

Vertical wind speed **Sonic temperature**

Fig. 8. Wavelet power spectra of the vertical wind speed **(a)** and sonic temperature **(b)** from 05:00–13:00 UTC (480 min) for COPS IOP8b at Fußbach. The period of free convection in the morning hours from 07:35–08:40 UTC is indicated by the black dotted vertical lines. The results of a pointwise significance test (significance level: 0.95) performed by Monte Carlo simulations (1000 realizations) are also shown in the wavelet power spectrum plots marked by black solid lines. The cone of influence is visible as a black curved line in the upper part of both figures.
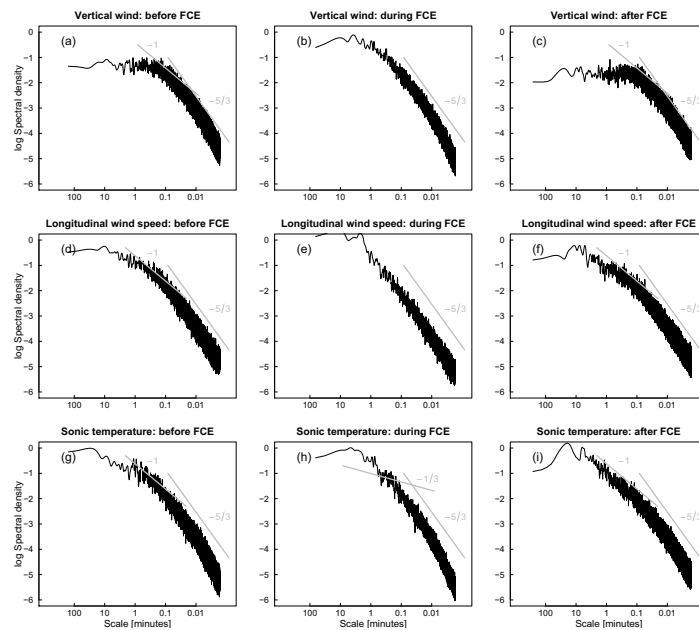
11407

Fig. 9. Power spectra of the vertical wind speed **(a–c)**, longitudinal wind speed **(d–f)** and sonic temperature **(g–i)**, before (05:00–07:35 UTC), during (07:35–08:40 UTC) and after (08:40–13:00 UTC) the FCE time for COPS IOP8b at Fußbach. The chosen time periods coincide with those distinguished in Fig. 8 by the black dotted vertical lines. The gray solid lines indicate the −5/3, −1 and −1/3 power laws.
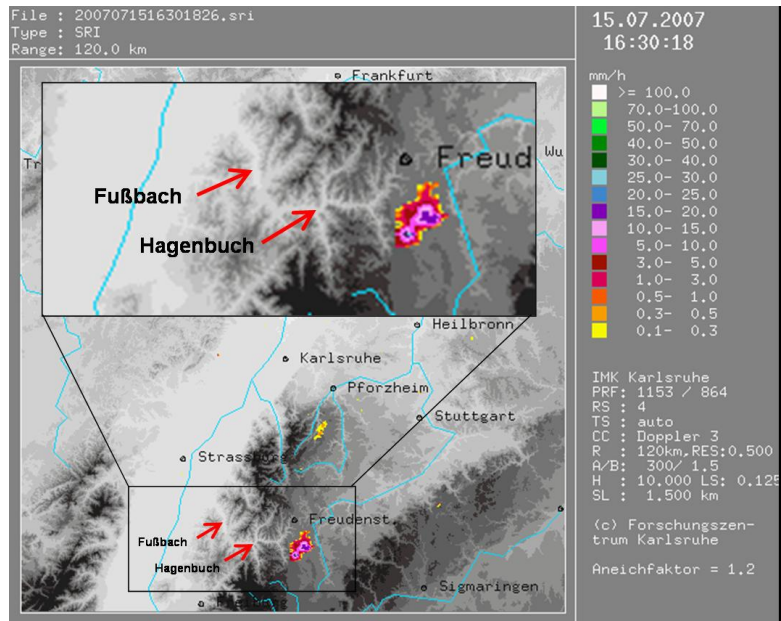
11408

Fig. 10. Radar image of the IMK-FZK (Institut für Meteorologie und Klimaforschung, Forschungszentrum Karlsruhe) Precipitation Radar archive for COPS IOP8b at 14:30 UTC. The image was obtained from the URL http://www.cops2007.de/ (last login: 16 March 2009; authorization required). The depicted rain rate $\left[\mathrm{mm\,h^{-1}}\right]$ reveals the formation of a single, precipitating cell at about 30 km south of Freudenstadt near the upper Kinzig valley. The location of the Fußbach site and another energy balance and turbulence station (Hagenbuch) installed by the University of Bayreuth in the Kinzig valley are indicated by red arrowheads. Both stations showed the occurrence of FCEs in the morning hours at COPS IOP8b.
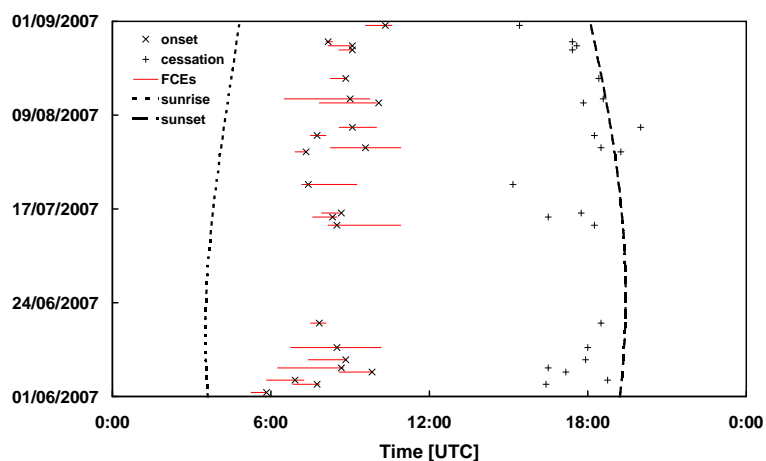
11409

Fig. 11. Onset and cessation times of the up-valley winds and the corresponding FCE periods in the morning hours at days classified as "event days" regarding the entire COPS measurement period at Fußbach. Also depicted are the times of sunset and sunrise.

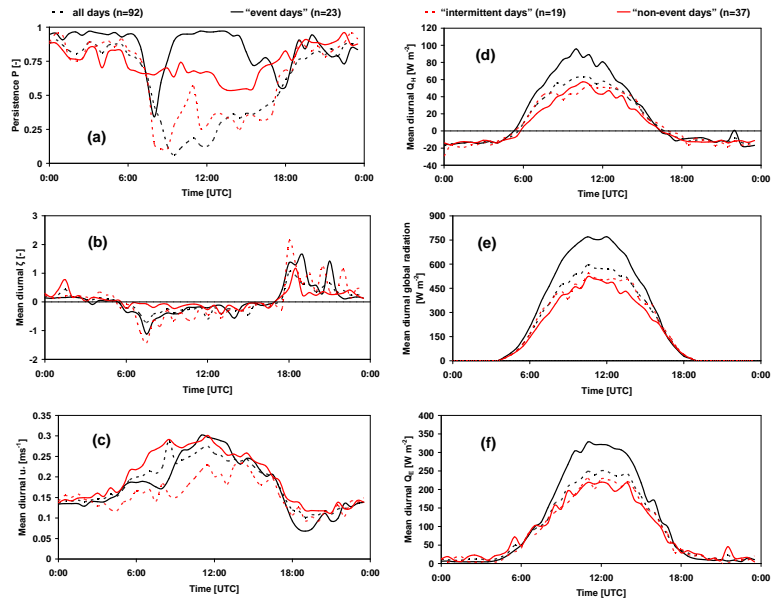**Fig. 12.** Persistence P [−] **(a)** and mean diurnal courses of the stability parameter ζ [−] **(b)**, friction velocity u_* $\left[\mathrm{m\,s^{-1}}\right]$ **(c)**, sensible heat flux Q_H $\left[\mathrm{W\,m^{-2}}\right]$ **(d)**, global radiation $\left[\mathrm{W\,m^{-2}}\right]$ **(e)** and latent heat flux Q_E $\left[\mathrm{W\,m^{-2}}\right]$ **(f)** for all days of the COPS measurement period (92), days classified as "event days" (23), "intermittent days" (19) and "non-event days" (37) at Fußbach. Thirteen days cannot be classified due to data failure.